Journal of Building Engineering 8 (2016) 48–57

Contents lists available at ScienceDirect

Journal of Building Engineering

journal homepage: www.elsevier.com/locate/jobe

Evaluation of thermal characteristics on a multi-sheet-type radiant panel heating system

Sihwan Lee [a], Beungyong Park [b], Jeongil Kim [c,*], Shinsuke Kato [d]

[a] Department of Architecture, Shinshu University, 4-17-1 Wakasato, Nagano city 380-8553, Japan
[b] Center for Building Energy Technology, Korea Conformity Laboratories, 7, Jeongtong-ro, Deoksan-myeon, Jincheon-gun, Chungcheongbuk-do 27872, Republic of Korea
[c] Energy and Environment Center, Misawa Homes Institute of Research and Development Co., Ltd, 1-1-19, Takaidonishi, Suginami-ku, Tokyo 168-0071, Japan
[d] Institute of Industrial Science, University of Tokyo, 4-6-1 Komaba Meguro-ku, Tokyo 153-8505, Japan

ARTICLE INFO

Article history:
Received 10 May 2016
Received in revised form
5 September 2016
Accepted 15 September 2016
Available online 16 September 2016

Keywords:
Radiant panel
Thermal environment
Heat transfer
U-value
Computational fluid dynamics (CFD)

ABSTRACT

The purpose of this study is to examine the thermal characteristics of a multi-sheet-type radiant panel heating system and its effect on the indoor thermal environment. To examine the thermal characteristics using computational fluid dynamic (CFD) simulations, simulation of a radiant panel model that considers actual usage condition combined with convection and radiation is very important. We analyze the indoor thermal environment of a real-scale space, heated by a radiant heating system, using full-scale measurement and CFD simulation. In a multi-sheet-type radiant panel, the convective heat transfer is greater than the radiative heat transfer. The multi-sheet-type radiant panel is actually not a real "radiant panel." It is named as such by the American Society of Heating, Refrigerating, and Air-Conditioning Engineers because its radiative heat transfer is more than 50%. We also determine the effects of indoor setup location of the radiant panel and panel shape on the heat-discharge characteristics. Compared with a single-sheet-type with the same heat discharge, a multi-sheet type has a larger surface area and area of contact with air. Thus, the convective heat transfer is greater, and the radiative heat transfer is smaller.

1. Introduction

To address the energy and environmental problems associated with global warming, increasing attention is being focused on the use of radiant heating systems combined with natural ventilation as energy-saving systems. Radiant heating systems such as floor, ceiling, wall, and panel heating systems are now regarded as energy efficient and comfortable heating systems compared with conventional heating systems [1–7]. The radiant heating system offers many advantages. It is more efficient than conventional air-conditioning system, and it directly delivers heat from the hot panel surface to the people skins and in the room via infrared radiation. Further, it does not produce noise or cause drafts and does not use ducts. Moreover, the system provides uniform temperature distribution, which is suitable for improving personal convenience. Hydronic (liquid-based) radiant heating systems can use a wide variety of energy sources to heat the liquid, including standard gas-fired boilers, oil-fired boilers, solar water heaters, geothermal heat pumps, or a combination of these sources. Additionally, many energy-efficient building technologies with increased thermal insulation and airtightness have also been applied in buildings with radiant heating systems, which could contribute to low building heat loss and reduce energy consumption [8].

The computational fluid dynamic (CFD) technology has been extensively used to predict indoor heat transfer and thermal comfort environment in a radiant panel heating system. Myhren and Holmberg [9] and Chen [10] discussed different heating systems using CFD simulations (a surface-to-surface radiation model and a low-Re number k–ε turbulence model) to investigate draught problems, differences in vertical temperature gradients, air-speed levels, and energy consumption in their work areas. Karadag et al. [11] used the standard k–ε turbulence model to study ceiling-panel systems. They found that when the room dimensions and temperature difference between the ceiling and interior air increase, the Nusselt number over the floor also increases. Song and Kato [12] performed a simple analysis of an indoor thermal environment of a radiant panel system using CFD simulation. They demonstrated that a hybrid air-conditioning system with a radiant panel system could realize better energy efficiency than ordinary systems in a hot and humid climate. However, verification using full-blown experiments has not been performed. In addition, although the radiant panels used were the multi-sheet-type in which thin panels were lined up to more

* Corresponding author.
E-mail address: jeongil_kim@home.misawa.co.jp (J. Kim).

http://dx.doi.org/10.1016/j.jobe.2016.09.006
2352-7102/

effectively exploit the dehumidifying effect of surface condensation, evaluation of the simulations was done using a simple model with a single sheet.

The CFD simulation must be verified through detailed modeling that simulates the actually used panel because this is the only means of accurately ascertaining the heat-discharge characteristics of a radiant panel while separating the radiated and convected heat components. In particular, multi-sheet-type panels have a useful function to adjust humidity environment that they easily cause surface condensation at a low surface temperature owing to their increased contact with air in the cooling mode. However, significant potential for a high level of convective heat transfer is expected due to the increase in the heat exchange area with air. Naturally, when panels consisting of multiple thin sheets are modeled using the CFD simulation, the calculated load increases with a finer mesh partition. However, with the present development in computer performance, this problem is not expected to be a major issue. To ascertain the heat-discharge characteristics of the panels, examining the heating operation at night is appropriate to eliminate the thermal load elements (solar radiation and latent heat) that complicate the simulation.

For the above reasons, the present study focused on a space heated by a radiant panel, and the heat-discharge characteristics of the radiant panel were ascertained by analyzing the room airflow and temperature distributions according to actual measurements and numerical analysis. Prediction precision sufficient for practical numerical analysis was confirmed for an indoor environment using a radiant panel by comparing and examining the results of both numerical analysis and actual measurement. This study also determines the extent to which the indoor setup location of the radiant panel and panel shape affect the heat-discharge characteristics of the radiant panel.

2. Experimental study

2.1. Full-scale room model description

Fig. 1 shows the space where the measurements were conducted [4.50 m (W) × 3.60 m (D) × 2.30 m (H)], which was in an experimental house at the Chiba Experiment Station (N 35° 36′ 18″, E 140° 7′ 24″), Institute of Industrial Science, University of Tokyo, Japan, as well as the radiant panel heating system. The west-side wall was connected to the adjoining preparation room, and the other walls were adjacent to the outside. In addition, the space has also two horizontal slider windows with dimensions of 1.60 m (W) × 0.80 m (H) and two vertical swing windows with dimensions of 1.60 m (W) × 0.40 m (H) in the north- and south-side walls. In the room, heating was provided using a multi-sheet-type radiant panel only [Table 1, two columns × 35 sheets (one sheet: 0.07 m (W) × 0.005 m (D) × 2.0 m (H); spacing distance between sheets = 0.035 m; spacing distance between columns = 0.02 m)]. The surface area of the radiation panel was 21.049 m^2, and 15 L/min of heated water was supplied to the radiation panel. No air inlet/outlet for ventilation or air conditioning was present. Thus, the only airflow in the room was natural convection due to buoyancy.

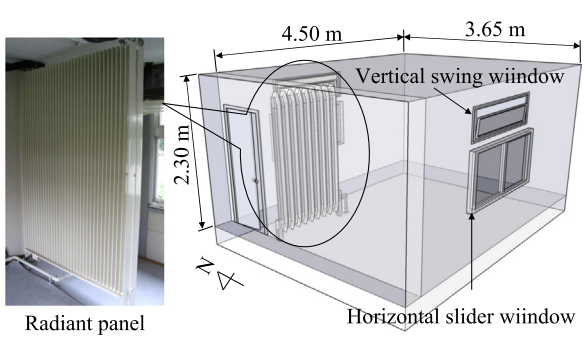

Fig. 1. Schematic room model with a radiant panel heating system.

Table 1
Specification of the multi-sheet-type radiant panel.

Item	Contents
Configuration of radiation panel	Two columns × 35 sheets (one sheet: 0.07 m (W) × 0.005 m (D) × 2 m (H)) Spacing distance between sheets: 0.035 m Spacing distance between columns: 0.020 m Size of flow path in a sheet: 0.068 × 0.003 m
Surface area of radiation panel	21.049 m^2
Supply water flow rate	15 L/min

2.2. Measurement of thermal insulation and infiltration performance in the room model

To determine the thermal insulation and infiltration performance from the cracks in the room model, the U-value of the walls and windows and the infiltration rate were measured. The measurement of the U-value (thermal transmittance) at the walls and windows was conducted using the infrared thermography method [13]. In the thermograph method, the heat flow through a component in contact with the outdoor air at a building site was calculated based on the indoor-side surface temperature (measured by an infrared camera), the total heat transfer coefficient, and the environmental temperature. Then, the U-value in a quasi-stationary state of the component was determined from the inside and outside environmental temperature difference. This method allows possible measurement of the insulation performance of the entire architectural component and demonstrate to the residents of the building the temperature distribution of the indoor walls in contact with the outdoor air. In addition, to determine the infiltration rate of the room model, tracer-gas measurement was used to quantify the infiltration rate on the natural ventilation state. The decay method, known as the step-down method, was used to calculate the infiltration rate through the cracks in the room because this method only requires relative concentrations; the tracer-gas injection rate need not be measured [14]. The infiltration rate was measured by uniformly dispersing sulfur hexafluoride (SF_6) as a tracer gas in the room. A desk fan in the room ensured proper mixing. Samples were drawn into a multi-gas monitor (INNOVA 1312) through plastic tubes at five different locations in the room at 30-s intervals. Eq. (1) was used to solve for I by periodically measuring the tracer-gas concentration during the decay and fitting the data in a logarithmic form. The ratio of airflow rate Q to volume V being tested has a unit of 1/time and considered as infiltration rate I [Eq. (2)] of the measured room.

$$C(t) = C_0 \cdot e^{-It} \tag{1}$$

$$I = \frac{Q}{V} \tag{2}$$

In these equations, t [h] is the time, C_0 [ppm] is the concentration of the tracer gas in the room at $t=0$, $C(t)$ [ppm] is the tracer-gas concentration at time t, I [h^{-1}] is the infiltration rate, Q [m^3/h] is the airflow rate out of the room, and V [m^3] is the room volume.

Table 2
Measurement items and their specifications.

Item	Contents
Vertical temperature distribution	T-type thermocouple [0.24-mm-diameter (from −200 to 300 °C), Sensitivity: approximately 43 μV/°C]
Surface of radiant panel and walls	T-type thermocouple
MRT	Globe thermometer (ANDO KEIKI Co., Ltd, CK-150, φ=150 mm)
	Hot-wire anemometer (KANOMAX Inc., Omnidirectional probe), Range: from 0.01 to 50.0 m/s; Resolution: 0.01 m/s [(0.01–9.99 m/s), 0.1 m/s (10.0–50.0 m/s)]
Outdoor air condition	Meteorological observation stations [VAISALA HMP45A probe (Pt100 resistance temperature detector (from −20 to 60 °C)), HUMICAP® 180 humidity sensor (from 0% to 100% RH non-condensing)]

2.3. Evaluation of indoor thermal environment

The evaluation of the indoor-thermal environment was obtained during winter. During the measurement, heated water was constantly supplied at a fixed temperature and flow rate (25 °C; 15 L/min), and the thermal environment in the room was evaluated during constant operation from February 1 to 11, 2010. To eliminate the effects of the thermal load due to solar radiation, results during nighttime (18:00 to 24:00) were investigated. Table 2 lists the measurement items and measurement equipment. To measure the vertical temperature distribution at the center of the room, seven t-type thermocouples were set up in a vertical array (height: 0.0, 0.4, 0.8, 1.2, 1.6, 2.0, and 2.3 m). The t-type thermocouple consists of copper and constantan, and it is suitable for measurements in the −200 to 350 °C range. To measure the mean radiant temperature (MRT), a globe thermometer (ANDO KEIKI Co., Ltd., φ=150 mm) and a hot-wire anemometer using omnidirectional probe (KANOMAX Inc.) were set up at a height of 1.2 m at the center of the room. Thermocouples were also installed on each wall and window, and the wall surface temperatures were monitored. In addition, outdoor air condition was monitored using meteorological observation stations.

2.4. Measurement results in full-scale room model

2.4.1. U-values and infiltration performance

Fig. 2 shows the wall and window surface temperature distributions measured using the infrared thermograph method, and Table 3 lists the calculated U-values. The highest value of 6.33 W/(m^2 K) was obtained at the windows, and the values at the walls, ceiling, and floor were 1.35, 2.73, and 0.82 W/(m^2 K), respectively. Moreover, the measurement result obtained by the tracer-gas method at the air leakage state is shown in Fig. 3. The infiltration rate in the room model was found to be 0.63 h^{-1} for the natural ventilation state. The room volume was 37.78 m^3. The airflow rate outside the room was calculated to be approximately 23.87 m^3/h for the natural ventilation state.

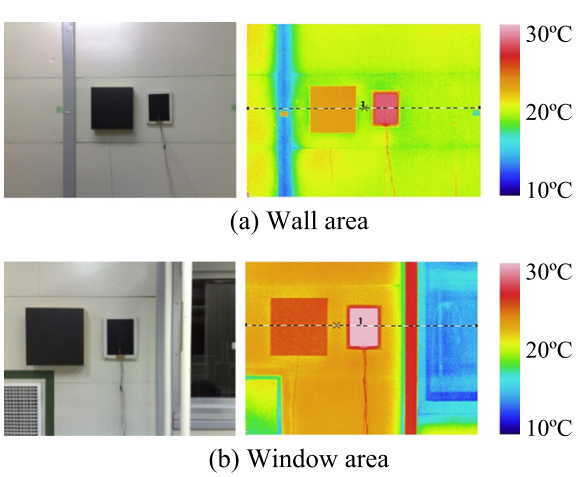

Fig. 2. Measured surface temperature by infrared thermography.

Table 3
Measured U-values.

Item	U-value
Wall	1.35 W/(m^2 K)
Ceiling	2.73 W/(m^2 K)
Floor	0.82 W/(m^2 K)
Window	6.33 W/(m^2 K)

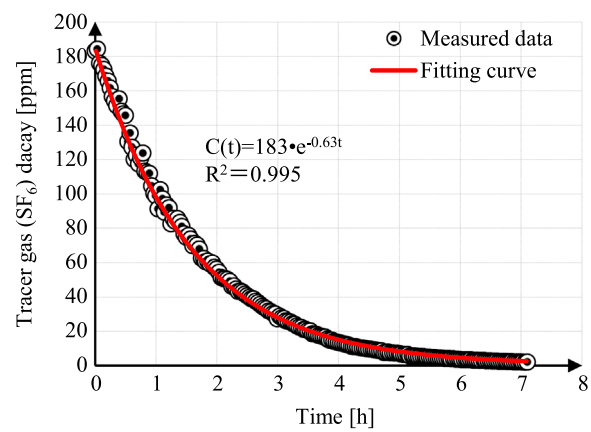

Fig. 3. Measured result obtained by the tracer-gas method on air leakage state.

2.4.2. Measurement results of indoor thermal environment

Fig. 4 shows the variation over time in the room and outdoor air temperature during measurement, surface temperature of the radiant panel [Fig. 4(a)], and the heat flux from the radiant panel, supply/return water temperature [Fig. 4(b)]. The heat flux from the radiant panel was calculated using the relationship of the supply/return water temperature and supply water flow rate using Eq. (3).

$$q = \rho \cdot C_p \cdot Q \cdot (T_s - T_r) \tag{3}$$

In this equation, q is the heat flux from the radiant panel to the indoor area, ρ is the water density, C_p is the specific heat of water, Q is the supply water flow rate, T_s is the supply water temperature, and T_r is the return water temperature.

Fig. 4(a) shows the surface temperature of the radiant panel and the variation over time in the room and outdoor air temperature. The surface temperature of the radiant panel fluctuated in the range of 23.0–23.7 °C. The room temperature fluctuated in the range of 15.0–15.8 °C and was below the recommended setting temperature of 20 °C for heating. Water at 25 °C was made to pass through the panel, and even with a maximum heating capacity of 1500 W, raising the room air temperature to 20 °C or higher was not possible. Because not much variation occurred in the outdoor air temperature, variation in the room air temperature was also small. Fig. 4(b) shows the heat flux from the radiant panel and

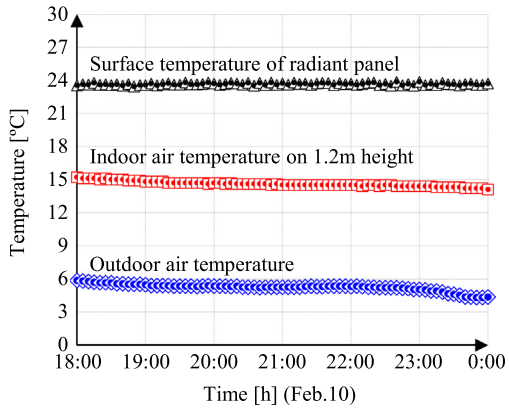

(a) Surface temperature of the radiant panel, indoor air temperature, and outdoor air temperature

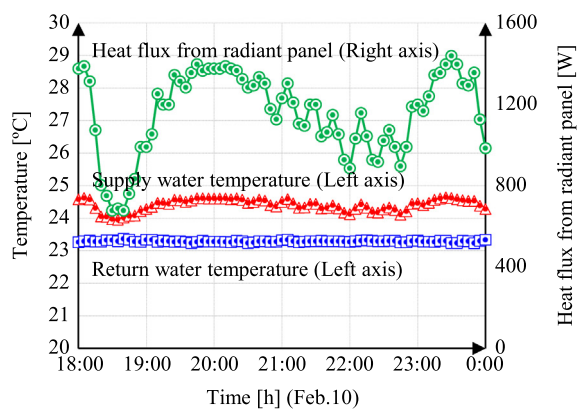

(b) Heat flux from the radiant panel and supply/return water temperature

Fig. 4. Measurement results during nighttime (18:00 to 24:00) on February 10, 2010.

supply/return water temperature. Because the heat flux from the radiant panel was affected by the supply/return water temperature, the change in the supply/return water temperature is important to maintain constant heat flux. The change in the heat flux occurs when the measurement time is from 18:00 to 19:00. This is the reason for the change in the supply water temperature to maintain the set point temperature of 25 °C because the indoor or surrounding air temperature of the radiant panel decreases after sundown. In addition, the outdoor temperature began to drop at 23:00, and immediately thereafter, the heat flux of the radiant panel increased and then decreased a little at 24:00.

Fig. 5 shows the room vertical temperature distribution at 0:00 on February 11, 2010 (outdoor air temperature: 4.35 °C; radiant panel heat flux: 971 W). Overall, the room air temperature exhibited a value lower than 18 °C, and the load handling capacity of the radiant panel did not extend to the outdoor air temperature. In terms of the room air temperature, warm air from the radiant panel collected near the ceiling surface, and the air temperature near the ceiling was high. The vertical temperature difference was approximately 3.6 °C (12.8–16.4 °C), and because the measured space was enclosed by walls and the air was calm, we believed that air warmed by the radiant panel concentrated at the top of the room due to natural convection resulting from buoyancy. In particular, the effect of natural convection was likely strengthened due to the cold drafts from window surfaces, thereby creating a vertical temperature difference. The MRT at a height of 1.2 m (14.1 °C) exhibited a value 0.6 °C lower than the air temperature at

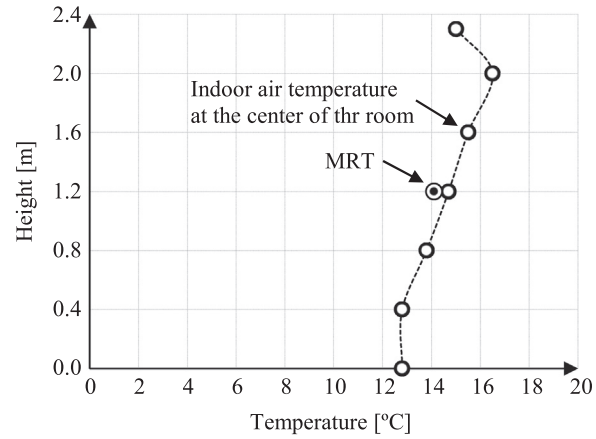

Fig. 5. Measured vertical temperature distribution and MRT at the center of the room.

the same height (14.7 °C), and we believed that air was heated due to convection in the room space from the radiant panel.

3. Numerical study

The numerically studied cases performed for the room model can be divided into three cases, as listed in Table 4. In Case 1, the model is validated by comparing the CFD simulation results with the experimental measurements, as presented in the previous section. In Case 2, the effect of radiant panel setup location was discussed, and in Case 3, the effect of radiant panel shape was discussed.

3.1. Overview of CFD simulation

To describe the flow in the room, a three-dimensional model was chosen. Fig. 6 shows the analyzed space, and Table 5 lists the solver setting and boundary conditions for the CFD simulation. A CFD model based on the finite volume method was used to simulate the temperature distribution in the room. A CFD program, STAR-CCM+(CD-adapco) [15], was used in this study, which is a commercially available and widely used tool incorporating several turbulence models. It is an implicit, segregated, and double-precision solver. The pressure–velocity coupling for the airflow field solution was represented using the Semi-Implicit Method for Pressure-Linked Equations algorithm [16]. The three-dimensional steady Reynolds-averaged Navier–Stokes equations were solved in combination with the low-Re number k–ε model. To improve the precision of the airflow/thermal analysis near the panel where a series of thin panels is present, the Abe–Kondoh–Nagano low-Reynolds number k-ε model was used [17,18]. This model is highly rated for its applicability to the reproduction of airflow (turbulence) near wall surfaces. In dealing with the buoyancy forces in the momentum equations, the Boussinesq approach was adopted, i.e., we assumed that the fluid properties are constant except for the density change with temperature, which gives rise to the buoyancy forces—this process is achieved using the linear

Table 4
Calculation cases.

Item	Description
Case 1	Model validation
Case 2	Effect of radiant panel setup location
Case 3	Effect of radiant panel shape

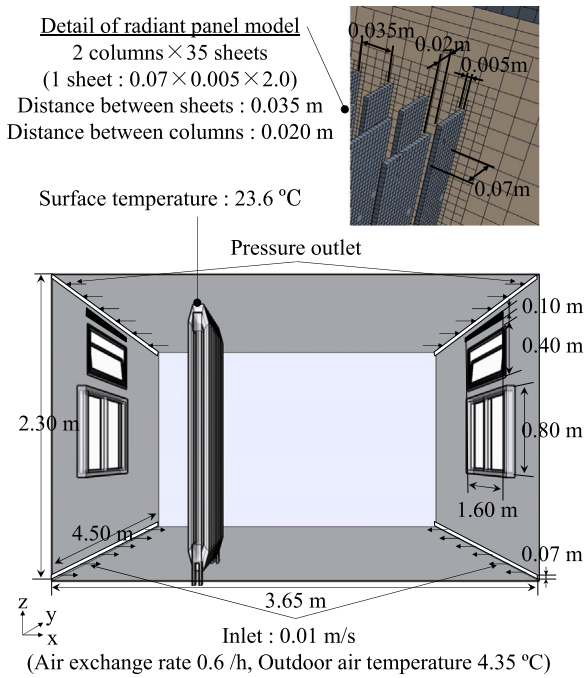

Fig. 6. CFD calculation model and detail of the radiant panel model.

Table 5
Solver setting and boundary conditions in the CFD simulation.

Item	Contents
Turbulence model	Low-Re number k–ε turbulence model (Abe–Kondoh–Nagano model)
Meshes	Approximately 2,000,000 cells (trimmed mesh), $y^+ < 1$, $\Delta x = 0.0005$–0.04 m
Time dependence	Steady state ($t = \infty$)
Buoyancy	Boussinesq approximation
Radiation calculation	Surface-to-surface radiation model, $\varepsilon_{all} = 0.8$, $\tau_{window} = 0.2$ ($\tau_{wall} = 0$)
Inlet	Defines the air draft on the floor Area: 2 EA × (4.50 (y) × 0.07 (z) m) = 0.63 m^2 $U_x = 0.01$ m/s (measured air exchange rate: 0.63 h^{-1}) $k = \frac{3}{2}(IU_x)^2$, $\varepsilon = \frac{C_\mu^{3/4} \cdot k^{3/2}}{L}$, $I = 0.1$, $L = 0.005$ m k: kinetic energy [m^2/s^2], I: turbulence intensity [-], L: length scale [m]
Outlet	Pressure outlet (U, k, ε: Free slip)
Walls, ceiling, floor, window	U-value: Table 3 Velocity: No-slip, $k|_{wall}$: No-slip, $\varepsilon|_{wall} = 2\nu(\frac{\partial\sqrt{k}}{\partial y})$

relationship between the density and temperature changes. The CFD simulation was combined with the radiation heat transfer simulation and HVAC control in the room [19]. For the radiation calculation, the surface-to-surface radiation model [20,21] was used in which the radiant heat flux between two surfaces is calculated by finding the shape factor from a one-to-one geometrical relationship of the surfaces. The heat of the transmission was found by providing the outdoor air temperature and using a one-dimensional stationary calculation. For the outdoor air temperature, a value of 4.35 °C was provided from the time of measurement (0:00, February 11, 2010). The measured values obtained from the thermograph method were used as U-values of the walls, and the west wall where the adjacent preparation room was present (the wall surface close to the radiant panel) was assumed to be insulated. A 7-cm opening was provided and connected to the outside based on the assumptions that draft infiltration will occur from the corners of the floor and the drafts will flow out to the corners of the ceiling. The size of the inlet for infiltration was assumed to have a 7-cm opening because natural ventilation has no effect on the convective heat transfer in the room. However, a stationary heat transfer was assumed, and the thermal storage effects and latent heat were not taken into account. The radiant panel was a multi-sheet type in which 70 thin sheets with a thickness of 5 mm were lined up in two rows. A fine-mesh structure (trimmed mesh, approximately 2,000,000 cells) was adopted to carry out a precise numerical simulation. For local residuals of continuity, momentum, and turbulence, the absolute criterion for convergence was set to 10^{-4}, and that for the energy was set to 10^{-7}.

3.2. Model validation by the CFD simulation and the actual measurements

To validate the CFD simulation, the results of the full-scale measurements were compared with those of the CFD simulations in the same space to verify that the CFD model result was consistent with the actual findings. The measurement data from 0:00 on February 11, 2010 were considered as the boundary condition. The measured outdoor air temperature, U-values of the walls, and infiltration rate were used as the boundary condition for the CFD simulation. In addition, a stationary state was assumed. Letting the room air temperature and room surface temperatures be unknown quantities, a coupled simulation of the convection and radiation was carried out to achieve a coupled calculation of the convective heat transfer (convective heat transfer of the room air with indoor surfaces and the radiant panel surface) and radiative heat transfer (radiative heat transfer among the indoor surfaces and between the radiant panel and indoor surfaces). Here, a comparison was made with the measurement results to examine the reliability of the CFD simulation model. Further, the radiant panel surface temperature was set to 23.6 °C, which is the same as the actual measured value.

3.3. Evaluation of thermal characteristics with radiant panel setup location and shape

Using a validated CFD simulation model, this study was conducted to evaluate the changes in the room thermal environment in relation to the setup location and shape of the radiant panel. Fig. 7 and Table 6 show the examined cases with the setup location and shape of the radiation panel.

3.3.1. Effect of radiant panel setup location

Case 1 is the simulation case for model validation as presented in the previous section. In Case 1, the windows in the room faced the radiant panel, and their temperatures were lower than those of the surrounding walls. Thus, they likely affected the radiative heat transfer at the radiant panel. Therefore, the examined case with the setup location was conducted in different setup locations such as in Case 2. In Case 2, the space was the same as that analyzed in Case 1, but the setup location of the radiant panel was placed close to the wall at the side with an adjoining room with insulated conditions (hereafter called as insulation surface). The distance between the insulation surface and radiant panel was 10 cm. The boundary conditions in this simulation were the same as those described in Section 3.1. Here, stationary heat transfer was also assumed, and the thermal storage effects and latent heat were not taken into account.

3.3.2. Effect of radiant panel shape

The multi-sheet radiant panel likely increased the surface area and the area of contact with air, thereby affecting the room thermal environment. The amount of radiative heat transfer is

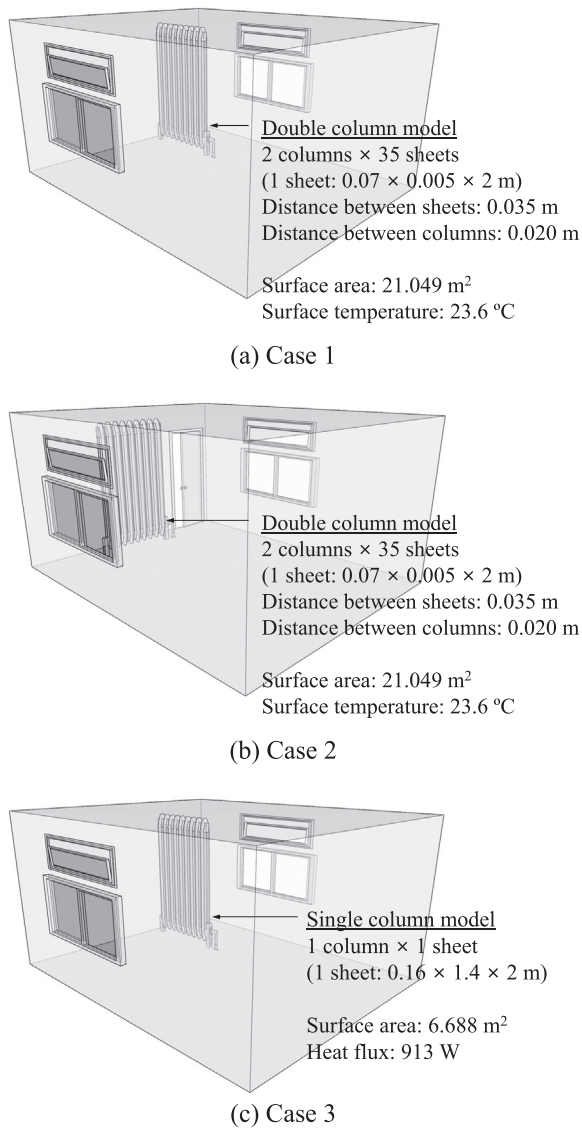

Fig. 7. Calculation cases with the setup location and shape of the radiation panel.

Table 6
Boundary conditions of the radiation panel with calculation cases.

Item	Cases 1 and 2	Case 3
Configuration of radiation panel	Double column model 2 columns × 35 sheets (1 sheet: 0.07 × 0.005 × 2 m) Distance of sheet: 0.035 m Distance of column: 0.020 m	Single column model 1 column × 1 sheet (1 sheet: 0.16 × 1.4 × 2 m)
Surface area of radiation panel	21.049 m^2	6.688 m^2
Boundary condition of radiation panel	Surface temperature: 23.6 °C	Heat flux: 913 W (same as in Case 1)

determined by the shape coefficient and temperature difference between the radiator and the heated object. The radiant panel was a multi-sheet-type panel in which heat-discharge fins were densely lined up in parallel, and this configuration promoted a convective heat transfer more than a radiative heat transfer. Therefore, the examined case with the panel shape was conducted using a simple panel such as in Case 3. In Case 3, the analysis space and setup location of the radiant panel were the same as those in Case 1. Case 1 simulated the shape of the radiant panel actually used, and in Case 3, the shape of a simple panel with only one sheet is used. The surface areas in Cases 1 and 3 differed, and thus, according to the surface boundary condition of the radiant panel in Case 3, the amount of heat provided (913 W) was equal to that obtained when the heat balance in Case 1 was determined. The boundary conditions in this simulation were the same as those described in Section 3.1. Here, stationary heat transfer was also assumed, and the thermal storage effects and latent heat were not taken into account.

4. Results and discussions

4.1. Model validation

4.1.1. Airflow vectors

Fig. 8(a) shows the airflow vectors in a cross section ($y = 1.46$ m) that cut through the room window surface and the radiant panel. Near the radiant panel, a rising flow of warm air appeared (maximum of 0.5 m/s), which resulted in the formation of a circulating flow. The air velocity near the ceiling was much faster than that in the other regions and exhibited a value of approximately 0.1 m/s. A downward airflow appeared near the window glass. The overall air velocity in the room region was low, i.e., 0.1 m/s or less.

4.1.2. Temperature distribution

Fig. 8(b) shows the room air temperature distribution in a cross section ($y = 1.46$ m) that cut through the room window surface and the radiant panel. Overall, the temperatures in the room were stratified. Near the floor, a relatively low temperature was observed due to the cold air from the window surfaces and drafts on the floor. Warm air from the radiant panel rose, and the air temperature at the top of the room reached approximately 18 °C for a temperature difference of approximately 6 °C between the top and

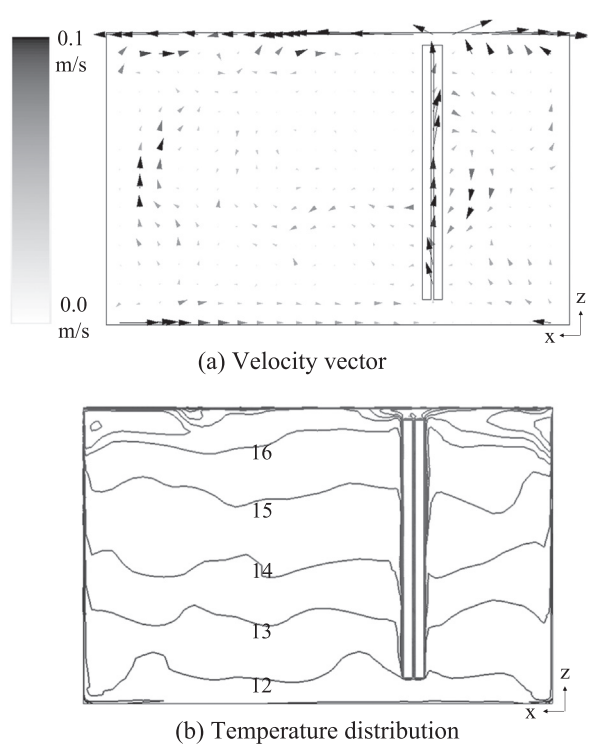

Fig. 8. CFD results of Case 1.

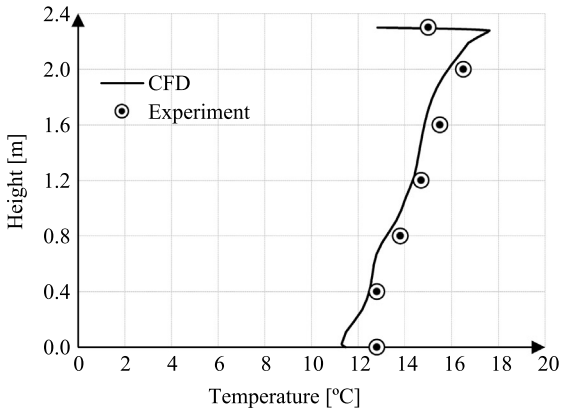

(a) Vertical temperature

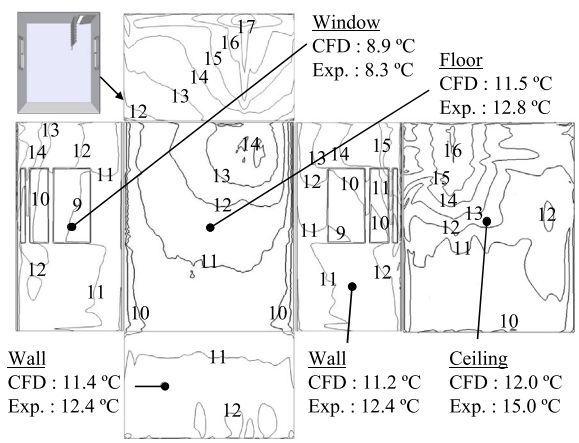

(b) Surface temperature

Fig. 9. Comparison of the experimental and CFD simulation results.

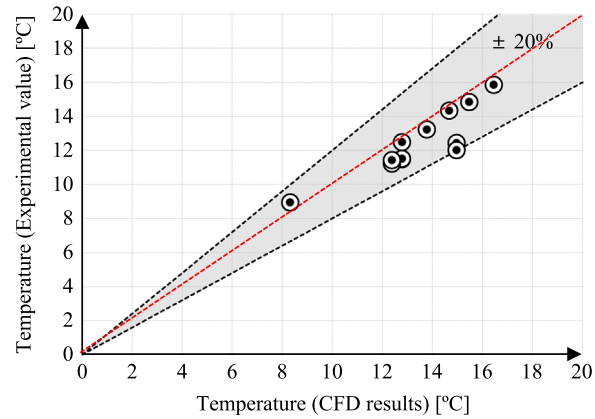

Fig. 10. Relative errors between of the experimental and CFD simulation results.

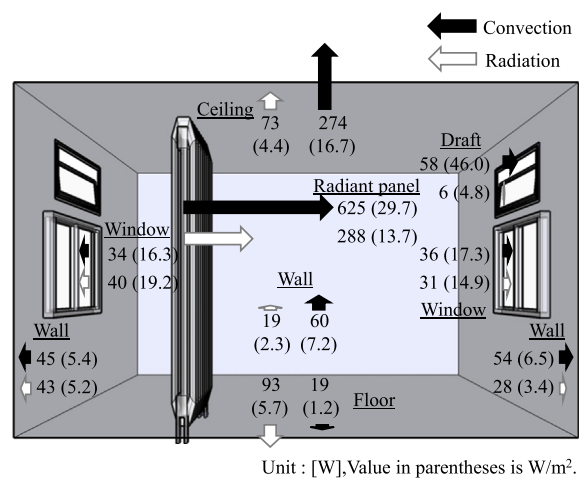

Fig. 11. Calculated heat flux of convection and radiation in Case 1.

bottom.

In addition, Fig. 9(a) shows the vertical temperature distribution at the center of the room, and Fig. 9(b) shows the wall surface temperatures in the indoor space. The floor surface temperatures were approximately 14–16 °C near the radiant panel, 11–14 °C in the other regions, and 11 °C or less in the corner areas where the drafts flow in. The calculated values for the wall surface temperatures were lower than the measured values, and the window glass surface temperature was higher than the measured values. In addition, although there was a resemblance in the gradient of the vertical temperature distribution, the overall calculated values were approximately 0.5 °C lower than the measured values, and a particularly marked difference in temperature existed between the floor and ceiling surfaces. The possible reasons for this discrepancy include the overly large wall surface U-values measured in the experiments and the error in the airtightness measurement. Another possible factor is the fact that the calculation error in the radiation calculation model, sash drafts, and thermal bridges were not taken into account in the analysis.

The relative errors between the experimental and CFD simulation results are shown in Fig. 10. All relative errors were $<20\%$; thus, the simulation model is sufficiently accurate to evaluate the thermal characteristics of the radiant heating panel.

4.1.3. Heat balance among walls

To confirm the large convection effects on the results of the measurement and simulation, the heat balance at the radiant panel and each wall surface was checked. Fig. 11 shows the heat balance at each wall surface relative to the heat discharged from the radiant panel. Warm air heated by the radiant panel accumulated near the ceiling, and the amount of heat transmitted from the ceiling was the largest. The windows were opposite to the radiant panel and had a lower temperature than the surrounding walls. Therefore, the amount of radiative heat transfer using the radiant panel was large, and the radiation component accounted for 54% of the transmitted heat loss.

In the radiant panel case, 32% (total heat flux: 913 W; convective heat flux: 625 W; radiative heat flux: 288 W) of the total heat flux handled the heating load through radiation. We believed that this is due to the multi-sheet-type, which was composed of multiple thin panels lined up in series that increased the surface area in contact with the air and thus boosted the convection effects. The American Society of Heating, Refrigerating, and Air-Conditioning Engineers uses the term “radiant panels” in cases where the amount of radiative heat transfer constitutes 50% or more of the overall heat transfer of a panel [22]. In this sense, the system used for the measurements is technically not a radiant panel system.

4.2. Effect of radiant panel setup location

4.2.1. Airflow vectors

The airflow distribution in Case 2 is shown in Fig. 12(a). Rising airflow occurred near the radiating panel, and near the ceiling, air flowed in the direction away from the radiant panel. In Case 2, a circulating flow occurred near the ceiling between the radiant panel and the insulation surface. We believed this is due to the proximity of the radiant panel to the insulation surface, and the

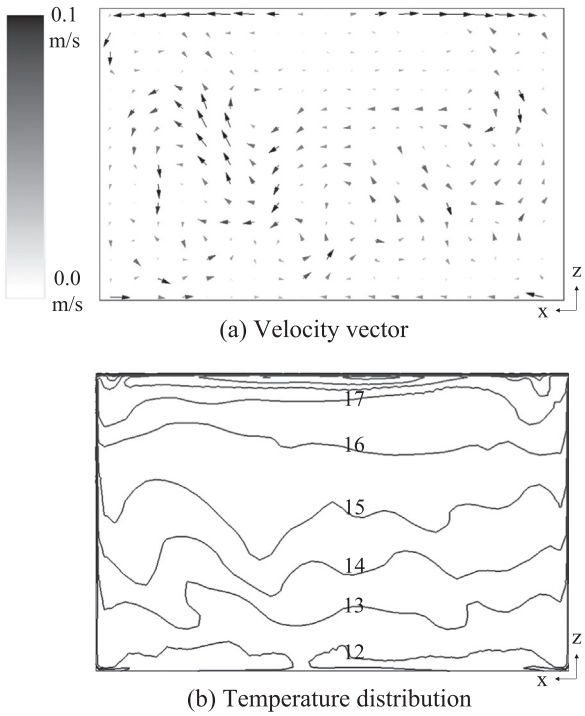

Fig. 12. CFD results of Case 2.

airflow, which rose near the panel, fell along the insulation surface. In almost all regions inside the room, the velocity was at or below 0.1 m/s. Overall, the room air velocity in Case 2 was greater than that in Case 1.

4.2.2. Temperature distribution

Fig. 12(b) shows the temperature distribution in Case 2. Overall, the temperatures in the room were stratified. Compared with Case 1 shown in Fig. 8(b), Case 2 exhibited a higher room air temperature, and referring at the temperature distribution at $x=2.25$ m in Case 2, air warmed by the radiant panel formed isotherms at almost constant heights up to the wall on the opposite side, Thus, the insulation surface near the radiant panel was likely totally warmed, which affected the thermal environment in the room.

Fig. 13(a) shows the vertical temperature distribution at the center of the room. Overall, Case 2 was approximately 0.5 °C higher than Case 1. The difference was largest near the ceiling (1.5 °C), which is likely because the rising airflow created by the radiant panel was transmitted to the opposite wall surface direction. The wall surface temperatures for Case 2 in the room space are shown in Fig. 13(b) [for Case 1, see Fig. 9(b)]. The temperature was higher at the insulation surface near the radiant panel [the wall surface at the top in Fig. 13(b)] in Case 2 than in Case 1. At the ceiling surface, the distribution of the isotherms was also greater than in Case 1. The temperature was also higher than in Case 1 at the wall surface where the insulation surface and radiant panel faced each other [wall surface at the bottom in Fig. 13(b)]. We believed that in Case 1, the cold window surface and the radiant panel stood opposite each other, and thus, a large heat loss occurred compared with that in Case 2. On the other hand, in Case 2, the radiant panel and the insulating surface faced each other at close range; thus, the wall surface was warmed, which consequently affected the room thermal environment.

At the point of comfortable indoor climate, the air temperature difference between the head and feet was approximately 2.6 °C (height = 0.1 m: 12.0 °C; height = 1.1 m: 14.6 °C). The radiant temperature asymmetry of the ceiling was 1.2 °C (room air

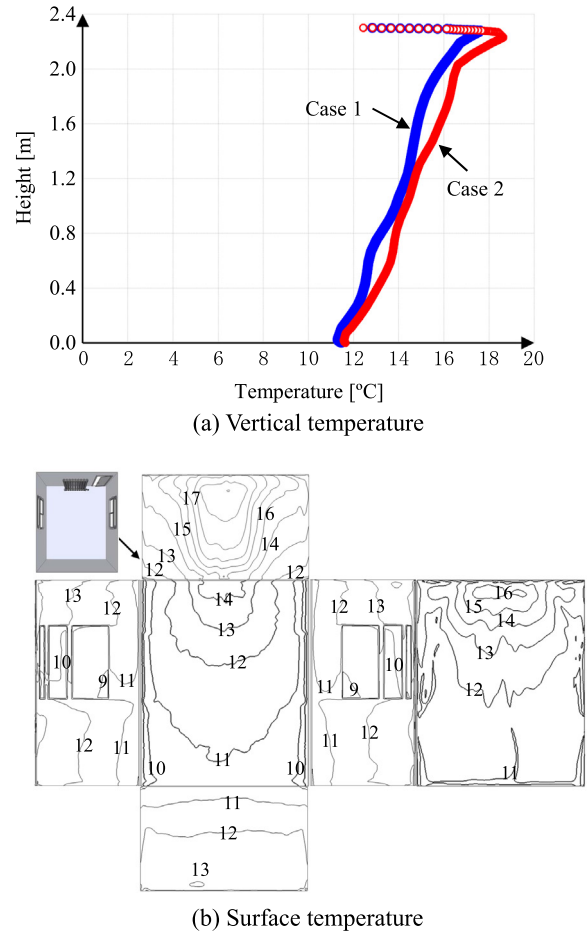

Fig. 13. Comparison of Cases 1 and 2 with respect to the vertical temperature and surface temperature in Case 2.

temperature = 14.7 °C; ceiling: 13.5 °C). The radiant temperature asymmetry of the windows was 5.2 °C (room air temperature = 14.7 °C; window: 9.5 °C). The recommended vertical air temperature for local thermal comfort was satisfied (< 3 °C) from ISO 7730 [23]. The recommended radiant temperature asymmetry of the windows (< 10 °C) and ceiling (< 5 °C) was also satisfied. We can confirm that thermal conditions can be ensured in the occupied room.

4.3. Effect of radiant panel shape

4.3.1. Airflow vectors

Fig. 14(a) shows the airflow vectors at $y=1.46$ m in Case 3 [for Case 1, see Fig. 8(a)]. In both cases, a rising airflow occurred near the radiant panel, and air flowed in the direction away from the radiant panel near the ceiling. The airflow velocity near the radiant panel ceiling was slower than that in Case 1, which we believed was due to the large surface area of the multi-sheet type panel that increased the area in contact with air and reinforced the effect of natural convection. In almost all regions in the room, the velocity was 0.1 m/s or less. Overall, the room air velocity was slower in Case 3 than in Case 1.

4.3.2. Temperature distribution

Fig. 14(b) shows the temperature distribution at $y=1.46$ m in Case 3 [for Case 1, see Fig. 8(b)]. Overall, the temperatures in the room were stratified. Compared with Case 1, the isotherms in Case 3 were wider, and the isotherm density in the high-temperature layers was greater. We believed this to be caused by the natural

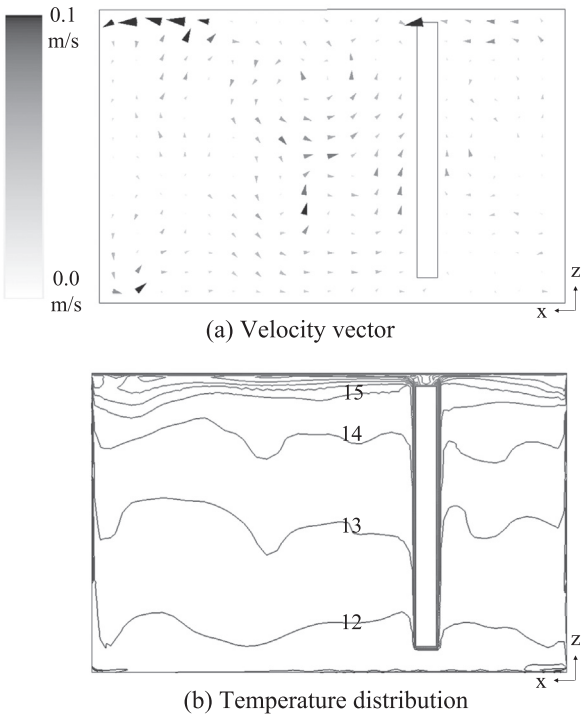

Fig. 14. CFD results of Case 3.

convection in the vertical direction of a multi-sheet panel, which was more active than that in the single-sheet type and affected the top part in the room, thus warming the air collected at the top of the room in Case 3.

Fig. 15(a) shows the vertical temperature distribution at the center of the room. Judging from the temperature gradient, the temperature difference between the top and bottom was smaller in Case 3 than in Case 1, which we believed to be due to the smaller effect of the natural convection in the indoor space than in Case 1. Fig. 15(b) shows the wall surface temperature in the room space in Case 3 [for Case 1, see Fig. 9(b)]. The temperature at the insulation surface close to the radiant panel [wall at the top in Fig. 15(b)] was higher in Case 3 than in Case 1 possibly because the amount of heat radiated by the radiant panels was set to the same value in each case. Using the single-sheet type with a small surface area and a small area in contact with air, the convective heat transfer was small, and the radiative heat transfer was large, which increased the wall surface temperature. Moreover, the air temperature difference between the head and feet was roughly 1.4 °C (height = 0.1 m: 11.5 °C; height = 1.1 m: 12.9 °C). The radiant temperature asymmetry of the ceiling was 1.5 °C (room air temperature = 12.9 °C; ceiling: 14.4 °C). The radiant temperature asymmetry of the windows was 2.9 °C (room air temperature = 12.9 °C; window: 10.0 °C). The recommended vertical air temperature for local thermal comfort was satisfied (< 3 °C) from ISO 7730 [23]. The recommended radiant temperature asymmetry of the windows (< 10 °C) and ceiling (< 5 °C) was also satisfied. Increasing the surface temperature has been shown to reduce the potential cold thermal discomfort.

4.3.3. Heat balance among wall surfaces

Fig. 16 shows the heat balance at each wall in Case 3, and Fig. 17 shows the convection and radiation components of the heat released by the radiant panel. The heat released by the radiant panel due to radiation was greater in Case 3 than in Case 1. Of the heat released by the radiant panel, 57.8% (total heat flux: 913 W; convective heat flux: 385 W; radiative heat flux: 528 W) of the heat transfer was due to radiation, and this affected each wall surface.

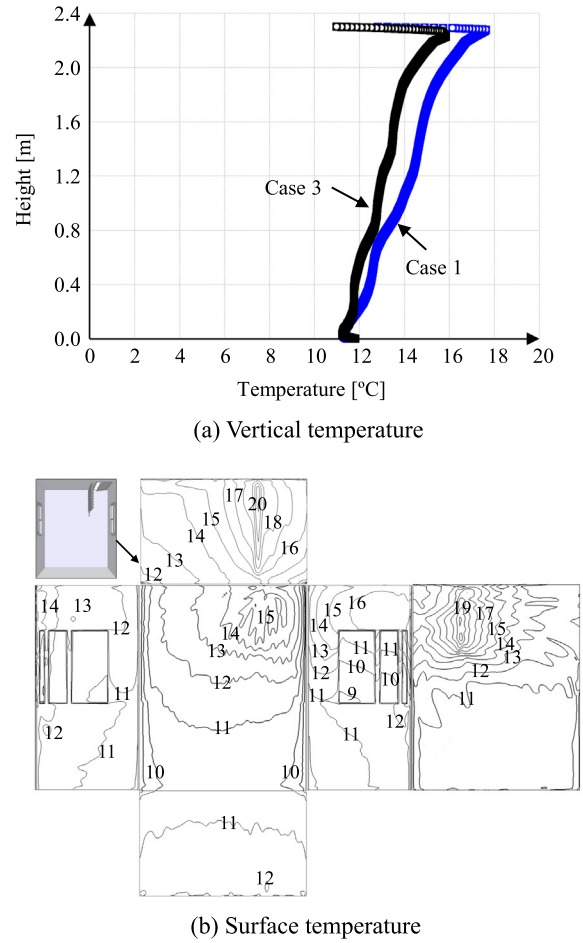

Fig. 15. Comparison of Cases 1 and 3 with respect to the vertical air temperature and surface temperature in Case 3.

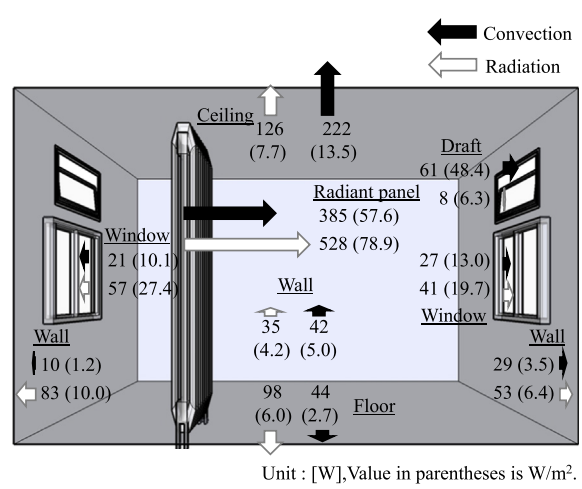

Fig. 16. Calculated heat flux of convection and radiation in Case 3.

The amount of radiative heat transfer was high at the wall with a window facing the largest side of the radiant panel, and this effect was particularly evident at the surface a short distance away [wall surface at the left side in Fig. 15(b)].

5. Conclusions

A multi-sheet radiant panel shows significant potential for high level of convective heat transfer due to the increase in the heat

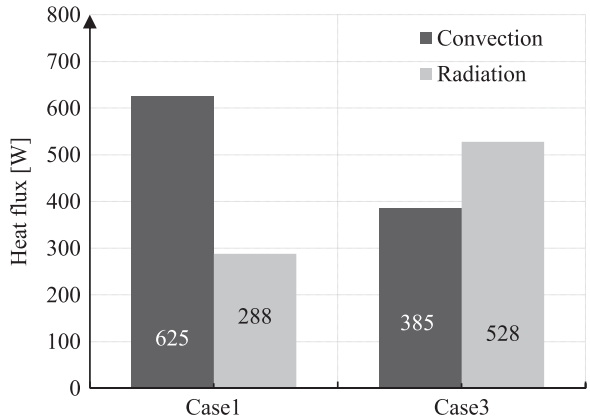

Fig. 17. Calculated heat flux from the radiant panel.

exchange area with air. In this study, the thermal characteristics of multi-sheet radiant panels were evaluated, and a comparison was made between full-scale measurement of an indoor thermal environment employing a radiant panel and analysis using CFD simulation. Further, the changes in the heat-discharge characteristics depending on the radiant panel setup location and shape were ascertained. The following results were obtained:

(1) We confirmed that the multi-sheet-type radiant panel has higher convective heat transfer, although the MRT at a height of 1.2 m (14.1 °C) exhibited a value 0.6 °C lower than the air temperature at the same height (14.7 °C).
(2) We confirmed through comparison of the CFD simulation and full-scale measurement results that the difference in terms of temperature was approximately 0.6–3.0 °C and that the prediction precision was adequate for practical use. In addition, the heat-discharge characteristics of the multi-sheet-type radiant panel were ascertained, and the results showed that approximately 68.5% of the total heat flux of the multi-sheet panel managed the heat load through convection.
(3) Changing the setup location of the radiant panel affects the indoor thermal environment. When the panel faces the insulation wall, it reduces the heat loss in the windows. The radiant panel could be placed in the wall-side positions to achieve increased indoor air temperature under the same heating surface temperature.
(4) Compared with a single-sheet-type with the same heat discharge, a multi-sheet-type with a series of thin panels has a larger surface area and area of contact with air; thus, the convective heat transfer is greater and the radiative heat transfer is smaller. We believe that it reduces the air contact area and limits the convective heat transfer. Therefore, the design for a radiant panel must consider investigating its thermal characteristics.

Conflict of interest

None declared.

Acknowledgments

This work was supported by the University of Tokyo, Japan.

References

[1] Richard Watson, Kirby Chapman, Radiant Heating and Cooling Handbook, McGraw Hill Professional, New York City, 2002.
[2] B.W. Olesen, Radiant floor heating in theory and practice, ASHRAE J. 7 (2002) 19–24.
[3] Jan Babiak, Bjarne W. Olesen, Dusan Petras, Low Temperature, Heating and High Temperature Cooling, REHVA, 2009.
[4] Robert Bean, Bjarne W. Olesen, Kwang Woo Kim, History of radiant heating and cooling systems, Part 1, ASHRAE J. 52 (2010) 40–47.
[5] Robert Bean, Bjarne W. Olesen, Kwang Woo Kim, History of radiant heating and cooling systems, Part 2, ASHRAE J. 52 (2010) 50–55.
[6] PRICE, Introduction to radiant heating and cooling, in: Proceedings of the Engineer's HVAC Handbook—A Comprehensive Guide to HVAC Fundamentals, Price Industries Limited, Winnipeg, MB, Canada, 2011.
[7] E.F. Helmut, Corina Stetiu, hydronic radiant cooling–preliminary assessment, Energy Build. 22 (1995) 193–205.
[8] Xiaozhou Wu, Bjarne W. Olesen, Lei Fang, Jianing Zhao, Fenghao Wang, Indoor temperatures for calculating room heat loss and heating capacity of radiant heating systems combined with mechanical ventilation systems, Energy Build. 112 (2016) 141–148.
[9] J.A. Myhren, S. Holmberg, Flow patterns and thermal comfort in a room with panel, floor and wall heating, Energy Build. 40 (2008) 524–536.
[10] Q. Chen, Comfort and energy consumption analysis in buildings with radiant panels, Energy Build. 14 (1990) 287–297.
[11] R. Karadag, I. Teke, H. Bulut, A numerical investigation on effects of ceiling and floor surface temperatures and room dimensions on the Nusselt number for a floor heating system, Int. Commun. Heat. Mass Transf. 34 (2007) 979–988.
[12] Doosam Song, Shinsuke Kato, Radiational panel cooling system with continuous natural cross ventilation for hot and humid regions, Energy Build. 36 (2004) 1273–1280.
[13] S. Kato, K. Kuroki, S. Hagihara, Method of in-situ measurement of thermal insulation performance of building elements using infrared camera, in: Proceedings of the 6th International Conference on Indoor Air Quality, Ventilation and Energy Conservation in Buildings, IAQVEC, 2007.
[14] ASHRAE Handbook - Fundamentals, Ventilation and infiltration, American Society of Heating, Refrigerating and Air-Conditioning Engineers (ASHRAE) Inc. 2011, pp. 16.5–16.6.
[15] STAR-CCM+ version 5.02 User Guide, CD-Adapco, 2010.
[16] S.V. Patankar, D.B. Spalding, A calculation procedure for heat, mass and momentum transfer in three-dimensional parabolic flows, Int. J. Heat. Mass Transf. 15 (10) (1972) 1787–1806.
[17] K. Abe, T. Kondoh, Y. Nagano, A new turbulence for predicting fluid flow and heat transfer in separating and reattaching flows - I. Flow field calculations, Heat. Mass Transf. 37 (1994) 139–151.
[18] K. Abe, T. Kondoh, Y. Nagano, A new turbulence for predicting fluid flow and heat transfer in separating and reattaching flows - II. Thermal field calculations, Heat. Mass Transf. 38 (1995) 1467–1481.
[19] S. Murakami, S. Kato, T. Kim, Indoor cooling/heating loads analysis based on coupled simulation of convection, radiation and HVAC control, Build. Environ. 36 (2001) 901–908.
[20] R. Siegel, J.R. Howell, Thermal Radiation Heat Transfer, 3rd ed., Hemisphere Publishing Co, 1992.
[21] R.P. Taylor, R. Luck, Comparison of reciprocity and closure enforcement methods for radiation view factors, J. Thermophys. Heat. Transf. 9 (1995) 660–666.
[22] ASHRAE Handbook - HVAC Systems and Equipment, Panel heating and cooling, American Society of Heating, Refrigerating and Air-Conditioning Engineers (ASHRAE) Inc. 2012, p. 6.1.
[23] ISO 7730, Ergonomics of the thermal environment — Analytical determination and interpretation of thermal comfort using calculation of the PMV and PPD indices and local thermal comfort criteria, 2005.